

Enhancement of Loop induced 125GeV Higgs pair production through Large-Extra-Dimensions model at the LHC

Sun Hao^{1*}, Zhou Ya-Jin^{2†}

¹ School of Physics and Technology, University of Jinan, Jinan, Shandong 250022, P.R.China

² School of Physics, Shandong University, Jinan, Shandong 250100, P.R.China

Abstract

Based on the analysis of 5 fb^{-1} of data at the LHC, the ATLAS and CMS collaborations have presented evidence for a Higgs boson with a mass in the 125 GeV range. We consider the 125 GeV neutral Higgs pair production process in the context of large-extra-dimensions(LED) model including the Kaluza-Klein(KK) excited gravitons at the LHC. We take into account the LED effects coming from gluon-gluon fusion and quark-antiquark collision channels as well as their corresponding next-to-leading order(NLO) QCD loop induced corrections. We analyse their impacts on both the total cross section and some key distributions. Indeed, $pp \rightarrow HH$ has the clear advantage of a lower standard model(SM) background compare to process like $pp \rightarrow jj$, though its SM prediction is very small, it is shown that the LED model raises the cross section of Higgs pair production compare to its SM prediction and enhance the transverse momentum(p_T^H) and invariant mass(M_{HH}) distributions especially at high scales of p_T^H and M_{HH} . By including the NLO QCD loop corrections, the scale dependence of total cross section can be reduced obviously. Choose suitable decay modes like $HH \rightarrow b\bar{b}\gamma\gamma$ or $HH \rightarrow b\bar{b}\mu^-\mu^+$ and some simple cuts, we can strongly reduce the SM background but keep most of the LED effects, leading Higgs pair production a promising channel to search LED effects.

KeyWords: Higgs Pair Production, NLO QCD Corrections, Large Hadron Collider(LHC)

PACS: 11.10.Kk, 12.38.Bx, 14.80.Bn

*haosun@mail.ustc.edu.cn

†zhouyj@sdu.edu.cn

I. Introduction

The hierarchy problem of the standard model (SM) strongly suggests new physics at TeV scale, and the idea that there exists extra dimensions (ED) which first proposed by Arkani-Hamed, Dimopoulos, and Dvali[1] might provide a solution to this problem. They proposed a scenario in which the SM field is constrained to the common 3+1 space-time dimensions (“brane”), while gravity is free to propagate throughout a larger multidimensional space $D = \delta + 4$ (“bulk”). The picture of a massless graviton propagating in D dimensions is equal to the picture that numerous massive Kaluza-Klein (KK) gravitons propagate in 4 dimensions. The fundamental Planck scale M_S is related to the Plank mass scale $M_{Pl} = G_N^{-1/2} = 1.22 \times 10^{19}$ GeV according to the formula $M_{Pl}^2 = 8\pi M_S^{\delta+2} R^\delta$, where R and δ are the size and number of the extra dimensions, respectively. If R is large enough to make M_S on the order of the electroweak symmetry breaking scale (~ 1 TeV), the hierarchy problem will be naturally solved, so this extra dimension model is called the large extra dimension model (LED) or the ADD model. Postulating M_S to be 1 TeV, we get $R \sim 10^{13}$ cm for $\delta = 1$, which is obviously ruled out since it would modify Newton’s law of gravity at solar-system distances; and we get $R \sim 1$ mm for $\delta = 2$, which is also ruled out by the torsion-balance experiments[2]. When $\delta \geq 3$, where $R < 1$ nm, it is possible to detect graviton signal at high energy colliders.

Both the ATLAS and CMS collaborations have reported a SM Higgs-like excess at around $M_H = 125$ GeV. If a SM-like Higgs particle is discovered in this particular mass range, an important additional test of the SM electroweak symmetry breaking sector is the measurement of the Higgs self-interactions. At hadron colliders, the pair production of Higgs bosons plays a distinctive role in understanding the Higgs mechanism[3]. As the triple self-coupling of Higgs particles is involved in such production thus provide the experimental reconstruction of the Higgs potential. Precise measurement of this coupling could therefore give more insight on the mechanism of electroweak symmetry breaking. Compared to that of a single Higgs boson production, the signal-to-background ratio could significantly improved. The invariant mass scale of the single Higgs production is fixed by the Higgs mass, of order only ~ 125 GeV. Thus their detection through heavy quark decay modes suffer from large QCD backgrounds. Further

more, the Higgs pair production can give various final states, depending on the decay modes of the Higgs boson. In the mass range of (120,130)GeV, the Higgs boson decay modes with the largest branching fractions are $H \rightarrow b\bar{b}$ and $H \rightarrow W^+W^-$. The most probable decay mode for a pair of Higgs bosons is $HH \rightarrow b\bar{b}b\bar{b}$. However, this mode is challenging to search for due to the fact that it is difficult to trigger on, and that it competes against the QCD multi-jet backgrounds that possess overwhelmingly large cross sections. In general, QCD backgrounds can be suppressed with the existence of leptons and missing energy. In the SM frame, the promising channels are $pp \rightarrow HH \rightarrow b\bar{b}\tau^+\tau^-(b\bar{b}\mu^-\mu^+, b\bar{b}\gamma\gamma)$ [4] and $pp \rightarrow HH \rightarrow b\bar{b}W^+W^-$ [5] for $M_H \sim 125$ GeV. More detail analysis can be found later.

Another important distinctive feature of the Higgs pair production at the LHC is that the effects of physics beyond the SM can remarkably enhance the cross section with respect to that of the SM. Phenomenological studies of Higgs pair production have thus been performed in the context of the fourth generation model[6], the littlest Higgs model[7] and the Universal Extra Dimensions model[8]. For the large extra dimensional models, the tree level diagrams mediated by the Kaluza-Klein gravitons lead to a large total cross section. Such new theoretical approaches have drawn extensive attention in ref[9] for a comparison between supersymmetry and LED models. Exchange of virtual KK graviton or emission of a real KK mode could give rise to interesting phenomenological signals at TeV scale[10, 11]. Virtual effects of KK modes could lead to the enhancement of the cross section of pair productions in processes, for example, di-lepton, di-gauge boson ($\gamma\gamma, ZZ, W^+W^-$), dijet, $t\bar{t}$ pair[12, 13, 14, 15, 16, 17] etc. Some of these calculations have also been expanded into NLO QCD loop level. A detailed calculation of Higgs pair production in LED model has been performed recently[18], however, the QCD loop induced calculation based on the LED context is still missing.

Experimentally, the CMS Collaboration has performed a lot of search for LED on different final states at $\sqrt{s} = 7$ TeV[19, 20, 21]. By combining the diphoton, dimuon and dielectron channels, lower limits are set on the effective Planck scale in the range of 2.3~3.8 TeV at the 95% confidence level[22]. These limits are the most restrictive bounds on virtual graviton exchange up to date. Based on the analysis of $5 fb^{-1}$ of data at the LHC, the ATLAS[23]

and CMS[24] collaborations have presented evidence for a Higgs boson with a mass in the 125 GeV range. We thus concentrate on the 125 GeV Higgs pair production related to the latest measurement with the effects of the LED models and find the characteristic distribution of it up to QCD loop induced level.

This paper is organized as follows: in section 2 we present a brief introduction to the related theory. in section 3 we present the main contribution to the process and section 3 is arranged to present the numerical results of our studies. Finally we summarize the results in the last section.

II. Related theories

The LED model consists of the gravity sector and the SM sector. The manifold which gravity propagates, is not the ordinary 4 dimensional spacetime manifold, but $R^4 \times M$, where M is a δ -torus with radius R and volume $V_\delta = (2\pi R)^\delta$ without loss of physical significance. In our calculation we use the de Donder gauge. The relevant Feynman rules involving spin-2 KK graviton and the relevant vertices in the LED model can be found in Ref[10, 11, 25].

We denote the process as:

$$pp \rightarrow ij \rightarrow G_{KK} \rightarrow HH + X(ij = q\bar{q} = u\bar{u}, d\bar{d}, c\bar{c}, s\bar{s}, b\bar{b}, gg) \quad (2.1)$$

where G_{KK} denotes the Kaluza-Klein(KK) gravitons. The couplings between gravitons and SM particles are proportional to a constant named gravitational coupling $\kappa \equiv \sqrt{16\pi G_N}$, which can be expressed in terms of the fundamental scale M_S and the size of the compactified space radius R by $\kappa^2 R^\delta = 8\pi(4\pi)^{\delta/2}\Gamma(\delta/2)M_S^{-(\delta+2)}$. In practical experiments, the contributions of the different KK modes have to be summed up, so the propagator is proportional to $i/(s_{ij} - m_{\vec{n}}^2)$, where $s_{ij} = (p_i + p_j)^2$ and $m_{\vec{n}}$ is the mass of the KK state \vec{n} . When the effects of all the KK states are taken together, the amplitude is proportional to $\sum_{\vec{n}} \frac{i}{s_{ij} - m_{\vec{n}}^2 + i\epsilon} = D(s)$. If $\delta \geq 2$ this summation is formally divergent as $m_{\vec{n}}$ becomes large. We assume that the distribution has a ultraviolet cutoff at $\Lambda \sim M_S$, where the underlying theory becomes manifest. Then $D(s)$ can be expressed as:

$$D(s) = \frac{1}{\kappa^2} \frac{8\pi}{M_S^4} \left(\frac{\sqrt{s}}{M_S}\right)^{\delta-2} [\pi + 2iI(M_S/\sqrt{s})]. \quad (2.2)$$

The imaginary part $I(\Lambda/\sqrt{s})$ is from the summation over the many non-resonant KK states and its expression can be found in Ref.[11]. Finally the KK graviton propagator after summing over the KK states is:

$$\tilde{G}_{KK}^{\mu\nu\alpha\beta} = D(s) \left(\eta_{\mu\alpha}\eta_{\nu\beta} + \eta_{\mu\beta}\eta_{\nu\alpha} - \frac{2}{D-2}\eta_{\mu\nu}\eta_{\alpha\beta} \right) \quad (2.3)$$

By adding all the Feynman rules in the LED model and the propagator given above, we can get the amplitudes(\mathcal{M}) for the SM and virtual KK graviton exchange contributions as well as their interferences. The cross section integral for hadron-hadron collisions can be written as

$$\sigma = \sum_{i,j} \int_{\tau_0}^1 \int_{\frac{\tau_0}{x_1}}^1 dx_1 dx_2 G_{i/p_a}(x_1, \mu_f^2) G_{j/p_b}(x_2, \mu_f^2) \cdot \int \frac{1}{\text{avgfac}} \frac{|\mathcal{M}_n(\hat{s} = x_1 x_2 s)|^2}{2\hat{s}(2\pi)^{3n-4}} d\Phi_n \quad (2.4)$$

where $G_{i,j/p_a,p_b}(x, \mu^2)$ represent the gluon or (anti)quark parton density functions, p_a, p_b indicate (anti)proton, μ_f is the factorization scale which can be chosen equal the renormalization scale μ_r when the loop calculation is included. $\frac{1}{\text{avgfac}}$ is the times of spin-average factor, color-average factor and identical particle factor. $|\mathcal{M}_n|^2$ presents the squared n-particle matrix element and divided by the flux factor $[2\hat{s}(2\pi)^{3n-4}]$. $d\Phi_n$ denotes the n-particle phase space differential. The quantity $\hat{s} = x_1 x_2 s$ is the effective center-of-mass(c.m.s.) energy, and the sum $\sum_{i,j}$ runs in case of quark-antiquark incident partons over all possible quark-antiquark combinations ($i, j = u, d, s, c, b, \bar{u}, \bar{d}, \bar{s}, \bar{c}, \bar{b}$). In case of gg initial state the sum has only one term with $i, j = g$. Typically the latest new parton distributions for collider physics CT10[26] has been used in our calculation.

The n-body phase space differential $d\Phi_n$ and its integral Φ_n depend only on \hat{s} and particle masses m_i due to Lorentz invariance:

$$\begin{aligned} \Phi_n(\hat{s}, m_1, m_2, \dots, m_n) &= \int d\Phi_n(\hat{s}, m_1, m_2, \dots, m_n) \\ &= \int \delta^4((p_i + p_j) - \sum_{k=1}^n p_k) \prod_{k=1}^n d^4 p_k \delta(p_k^2 - m_k^2) \Theta(p_k^0) \end{aligned} \quad (2.5)$$

with i and j denoting the incident particles and k running over all outgoing particles($k = 1, \dots, n$). In our calculation we use BASES[27] to do the phase space integration and Kaleu[28] to cross check with each other.

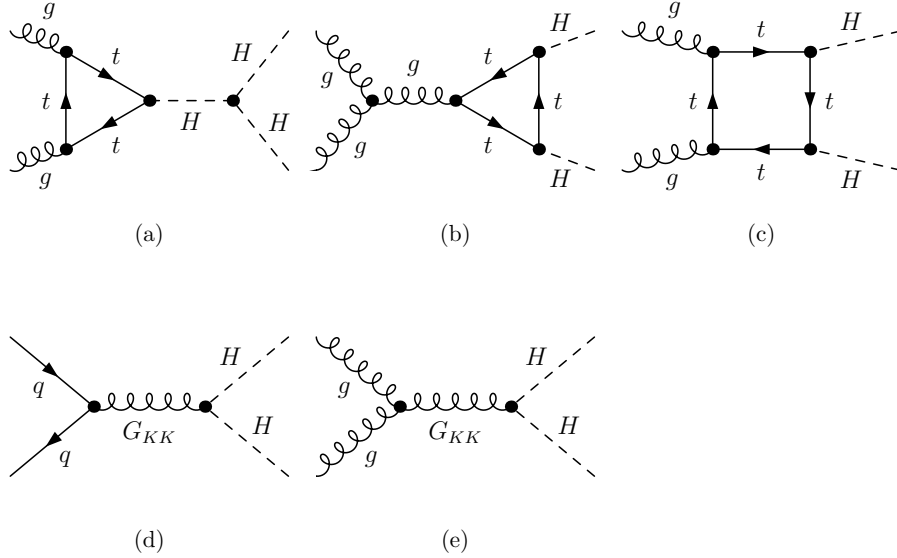


Figure 1: Part of Feynman diagrams for $pp \rightarrow HH$ in the SM (a, b, c) and the tree level quark-antiquark collision(d) and gluon-gluon fusion(e) diagrams in LED model, where q represents u-,d-,c-,s-, and b-quark while G_{KK} represents spin-2 KK graviton.

III. Related Process

We separate the total contributions into two parts. One is the pure SM effects and the other is the LED effects, simply denoted as σ^{SM} and σ^{LED} , respectively.

In SM, there is gluon-gluon fusion channel contribute to SM predictions through top-quark loops, see Fig. 1(a, b, c) for more details. There is also b-quark contribution, but it is small. Other diagrams include the change of the loop arrow in Fig.1(a, b, c) and cross change of the legs in Fig. 1(c) which are similar thus not shown, totally ten Feynman diagrams contribute. Contributions from the quark-antiquark collision can be safely omitted in the light fermion mass limits except b-b fusion through t-channels. However, it is only less of 0.5 percent of gluon-gluon fusion contribution[6], and not considered here. Thus we can define this contribution as $\sigma^{SM} = \sigma_{gg}^{SM_{LOOP}}$.

Now let's see the second part: contributions to the LED effects σ^{LED} . Several distinct contributions contribute to this part, include both the tree level and QCD loop induced level. We separate and highlight them into four different parts:

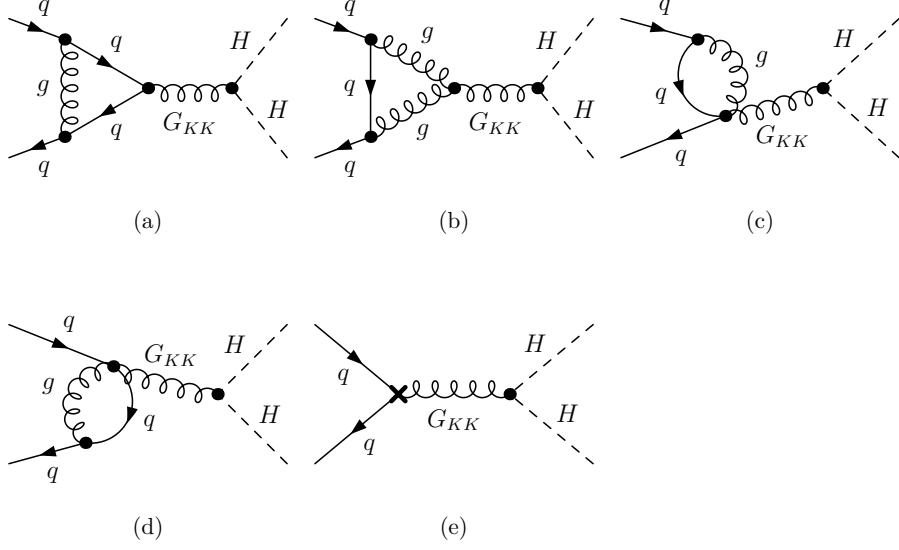


Figure 2: The QCD one-loop Feynman diagrams for the partonic process $q\bar{q} \rightarrow G_{KK} \rightarrow HH$ (a)-(d) and the counter term diagrams(e) correspond to Fig.1(d), where q represents u-,d-,c-,s-, b- and t-quark while G_{KK} represents spin-2 KK graviton.

- The tree level contributions defined as $\sigma_{q\bar{q},gg}^{LEDBORN}$ which include both the quark-antiquark collision and gluon-gluon fusion contributions, see Fig.1(d,e), directly connected by the effects of KK excitation of gravitons. There are two gravitational vertices thus such contributions are in the effective order $\mathcal{O}(\kappa^2)$.
- The $\mathcal{O}(\alpha_s)$ level one-loop virtual corrections to the leading order process as well as the renormalization of the leading order cross section which we define as $\sigma_{q\bar{q},gg}^{LEDBORN \otimes LEDLOOP}$. The QCD loop level Feynman diagrams of the quark-antiquark collision initial state part can be found in Fig.2, totally 4 loop diagrams and 1 counterterm diagram, while the gluon-gluon fusion contributions can be found in Fig.3 with 13 loop diagrams and 1 counterterm diagram as well. These contributions are in the effective order $\mathcal{O}(\kappa^2 \alpha_s)$.
- The SM one-loop prediction interference to the leading order process which defined as $\sigma_{gg}^{LEDBORN \otimes SMLOOP}$. These contributions are in the order $\mathcal{O}((\sqrt{\kappa}\alpha)\alpha_s)$. We keep these contributions for a fully consideration and it may also interesting to see how large are these contributions.
- Finally the real gluon and quark emission contributions. The Feynman diagrams can be found in Fig.4. The cross sections are defined as $\sigma_{q\bar{q},gg}^{REAL}$ which are also in the order

$\mathcal{O}(\kappa^2\alpha_s)$. We denote these parts by:

$$\begin{aligned}
(1) \quad & q(p_1)\bar{q}(p_2) \rightarrow G_{KK} \rightarrow H(p_3)H(p_4)g(p_5) \\
(2) \quad & q(p_1)g(p_2) \rightarrow G_{KK} \rightarrow H(p_3)H(p_4)q(p_5) \\
(3) \quad & g(p_1)\bar{q}(p_2) \rightarrow G_{KK} \rightarrow H(p_3)H(p_4)(\bar{q}(p_5))
\end{aligned} \tag{3.1}$$

and

$$\begin{aligned}
(1) \quad & g(p_1)g(p_2) \rightarrow G_{KK} \rightarrow H(p_3)H(p_4)g(p_5) \\
(2) \quad & q(p_1)g(p_2) \rightarrow G_{KK} \rightarrow H(p_3)H(p_4)q(p_5) \\
(3) \quad & g(p_1)\bar{q}(p_2) \rightarrow G_{KK} \rightarrow H(p_3)H(p_4)(\bar{q}(p_5))
\end{aligned} \tag{3.2}$$

refer to emission process related to quark-quark collision and gluon-gluon fusion sub-processes, respectively.

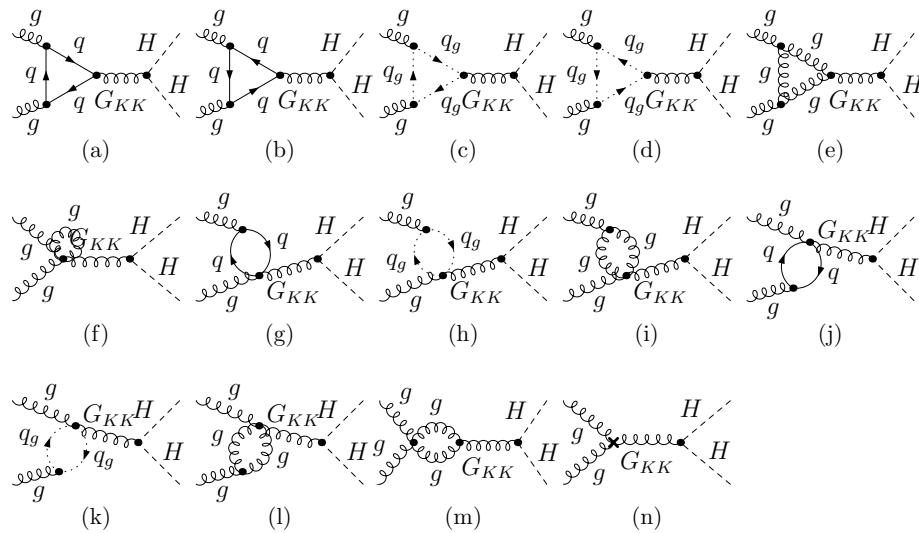


Figure 3: The QCD one-loop Feynman diagrams for the partonic process $gg \rightarrow G_{KK} \rightarrow HH$ (a)-(m) and the counter term diagrams(n) correspond to Fig.1(e), where q represents u-,d-,c-,s-, b- and t-quark while G_{KK} represents spin-2 KK graviton.

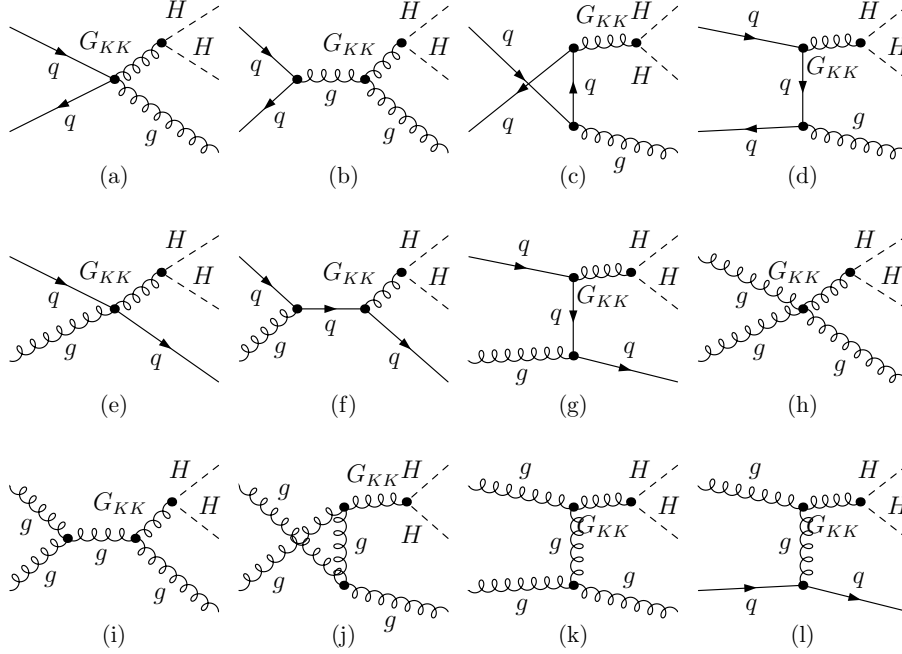


Figure 4: The tree-level Feynman diagrams for the real gluon/light-(anti)quark emission subprocess $q\bar{q} \rightarrow G_{KK} \rightarrow HHg$ related to Eq.3.2(1)[Fig.(a)-(d)], $q(\bar{q})g \rightarrow G_{KK} \rightarrow HHq(\bar{q})$ related to Eq.3.2(2,3)[Fig.(e)-(g)], $gg \rightarrow G_{KK} \rightarrow HHg$ related to Eq.3.3(1)[Fig.(h)-(k)], $gq(\bar{q}) \rightarrow G_{KK} \rightarrow HHq(\bar{q})$ related to Eq.3.3(2,3)[Fig.(l)], where q represents u, d, c, s, b and t -quark while G_{KK} represents spin-2 KK graviton.

Finally, we write the total cross section as sum of the above definitions to the formula below:

$$\sigma^{tot} = \sigma^{SM} + \sigma^{LED} \quad (3.3)$$

$$= \sigma_{gg}^{SM_{LOOP}} \quad (3.4)$$

$$+ \sigma_{q\bar{q}}^{LEDBORN} + \frac{\sigma_{q\bar{q}}^{LEDBORN \otimes LED_{LOOP}} + \sigma_{q\bar{q}}^{LED_{REAL}}}{\Delta\sigma_{q\bar{q}}^{LED}} \quad (3.5)$$

$$+ \sigma_{gg}^{LEDBORN} + \frac{\sigma_{gg}^{LEDBORN \otimes LED_{LOOP}} + \sigma_{gg}^{LEDBORN \otimes SM_{LOOP}} + \sigma_{gg}^{LED_{REAL}}}{\Delta\sigma_{gg}^{LED}} \quad (3.6)$$

$$= \sigma_{gg}^{SM_{LOOP}} + \sigma_{q\bar{q}}^{LED} + \sigma_{gg}^{LED} \quad (3.7)$$

$$= \frac{\sigma_{gg}^{SM_{LOOP}} + \sigma_{q\bar{q}}^{LED} + \sigma_{gg}^{LED}}{\sigma_{LO}} + \Delta\sigma_{q\bar{q}}^{LED} + \Delta\sigma_{gg}^{LED} \quad (3.8)$$

The reason to do this is to introduce the symbolic notations we use later and make it convenient for our numerical calculations. Eq.3.3 means we separate the total contributions into two parts. Eq.3.4 related to the SM contributions which include only UV and IR safe terms. Eq.3.5 and Eq.3.6 related to the quark-antiquark collision and gluon-gluon fusion contributions. Both are summed by two parts. One is the born level contributions the other are the loop induced LED contributions where we use $\Delta\sigma_{q\bar{q},gg}^{LED}$ to notate. We use $\sigma_{q\bar{q}}^{LED}$ and σ_{gg}^{LED} to keep

notation of Eq.3.5 and 3.6, respectively. Finally, we define the SM prediction plus the leading order LED contributions as σ^{LO} and the other terms are the shifted terms coming from the loop induced LED effects, see Eq.3.8.

There exist UV and soft/collinear IR singularities in the calculations of $\sigma_{q\bar{q},gg}^{LED_{BORN}\otimes LED_{LOOP}}$. To remove the UV divergences, we need only the wave function renormalization constants for the quark and gluon fields. We introduce the renormalization constants $\delta Z_{\psi_{q,L,R}}$ for massless quark (q=u,d,c,s,b) fields and δZ_A for the gluon field defined as

$$\psi_{q,L,R}^0 = (1 + \delta Z_{\phi_{q,L,R}})^{\frac{1}{2}} \psi_{q,L,R}, \quad A_\mu^{a0} = (1 + \delta Z_A)^{\frac{1}{2}} A_\mu^a \quad (3.9)$$

In the modified minimal subtraction (\overline{MS}) renormalization scheme the renormalization constants for the massless quarks are expressed as

$$\delta Z_{\psi_{q,L}} = -\frac{\alpha_s}{4\pi} C_F (\Delta_{UV} - \Delta_{IR}), \quad \delta Z_{\psi_{q,R}} = -\frac{\alpha_s}{4\pi} C_F (\Delta_{UV} - \Delta_{IR}), \quad (3.10)$$

$$\delta Z_A = \frac{\alpha_s}{4\pi} \left(\frac{5}{3} C_A - \frac{4}{3} n_f^{UV} T_F \right) \Delta_{UV} + \frac{\alpha_s}{4\pi} \left(\frac{5}{3} C_A - \frac{4}{3} n_f^{IR} T_F \right) \Delta_{IR}, \quad (3.11)$$

In the above equations μ_r is the renormalization scale, $C_F = \frac{4}{3}$, $C_A = 3$, $T_F = \frac{1}{2}$, $n_f^{UV} = 6$ corresponds to the six flavor quarks (u, d, c, s, t, b), whereas $n_f^{IR} = 5$ is the number of the massless quarks (u, d, s, c, b). Moreover, $\Delta_{UV} = \frac{1}{\epsilon_{UV}} \Gamma(1 + \epsilon_{UV}) (4\pi)^{\epsilon_{UV}}$ and $\Delta_{IR} = \frac{1}{\epsilon_{IR}} \Gamma(1 + \epsilon_{IR}) (4\pi)^{\epsilon_{IR}}$ refer to the UV and IR divergences, respectively.

By adding renormalization part to the virtual corrections, any ultraviolet(UV) singularities are regulated. Divergences arising from soft gluon emission removed by combining virtual and real emission corrections $\sigma_{q\bar{q},gg}^{LED_{REAL}}$. Singularities associated with initial state collinear gluon emission are absorbed into the definition of the parton distribution functions. We employ the \overline{MS} scheme for the parton distributions functions. Similar to the virtual part, we utilize dimensional regularization to control the singularities of the radiative corrections, which are organized using the two cutoff phase space slicing(TCPSS) method[29]. We adopt TCPSS to isolate the IR singularities by introducing two cutoff parameters δ_s and δ_c . An arbitrary small δ_s separates the three-body final state phase space into two regions: the soft region ($E_5 \leq \delta_s \sqrt{\hat{s}}/2$) and the hard region ($E_5 > \delta_s \sqrt{\hat{s}}/2$). The δ_c separates hard region into the hard collinear (HC) region and hard noncollinear (\overline{HC}) region. The criterion for separating the HC region is described

as follows: the region for real gluon/light-(anti)quark emission with \hat{s}_{15} (or \hat{s}_{25}) $< \delta_c \hat{s}$ (where $\hat{s}_{ij} = (p_i + p_j)^2$) is called the HC region. Otherwise it is called the \overline{HC} region. Then the cross section for each of the real emission partonic processes can be written as

$$\hat{\sigma}^R = \hat{\sigma}^S + \hat{\sigma}^H = \hat{\sigma}^S + \hat{\sigma}^{HC} + \hat{\sigma}^{\overline{HC}}. \quad (3.12)$$

After combining all these contributions above, the UV and IR singularities in σ^{tot} are exactly canceled. Dependence on the arbitrary small cutoff parameters δ_s and δ_c are exactly vanished. These cancelations can be verified numerically in our numerical calculations. We use Feynarts to create the amplitudes and FormCalc to perform the numerical calculation. To compute the one-loop tensor integrals we use our modified LoopTools [30, 31, 32] which supply an automatic numerical checks for the Infrared(IR) divergence and cross check with OneLoop[33] at enough random phase space points.

IV. Numerical results and discussions

In the SM frame, given the small total cross section, it is clear that even for $\sqrt{s} = 14$ TeV and a target luminosity of $\mathcal{O}(1000 fb^{-1})$ one need to focus on the Higgs decay channels with the largest branching ratios to visible final states to observe $pp \rightarrow HH + X$ such as $H \rightarrow b\bar{b}$ (59.48%), $H \rightarrow W^-W^+$ (20.78%) , $H \rightarrow \tau^-\tau^+(\mu^-\mu^+)$ (6.12%)[34]. A feasibility study on the decay channels $HH \rightarrow b\bar{b}\gamma\gamma$, $HH \rightarrow b\bar{b}\mu^-\mu^+$, finding that with $600 fb^{-1}$ one expects 6 signal and 11 background events, giving a significance of about 1.5σ [4]. For the channel $HH \rightarrow b\bar{b}W^-W^+ \rightarrow b\bar{b}l\nu jj$, Ref[5] claimed with 57 signal and 119 background events at $600 fb^{-1}$ by employing new techniques and assuming good τ reconstruction efficiency($\sim 80\%$), thus make such channel a promising one. As can be seen, though challenge, Higgs pair production in SM can be measured. What's more, we hope to concentrate on the Higgs pair production under LED frame and find out whether this production can be enhanced and given more chance to be tested.

In the numerical calculations, we take the input parameters as $M_Z = 91.1876$ GeV, $M_W = 80.399$ GeV[35], $\alpha(M_Z^2)^{-1} = 1/127.934$, $M_H = 125$ GeV[23, 24]. The factorization and renormalization scales are chosen to be the same $\mu_r = \mu_f = \mu_0 = M_H = 125$ GeV. Numerical analysis is done at the colliding c.m.s. energy 8TeV and 14 TeV LHC for the early and future LHC.

The UV and IR safeties are verified numerically after combining all the contributions at the QCD loop level. To check the UV and IR divergence cancelation, we display a random phase space point as well as the cancelation for different divergent parameters, see in Table1. One thing that should be emphasized is $\sigma_{q\bar{q},gg}^{LED_{BORN}\otimes LED_{LOOP}} + \sigma_{gg}^{LED_{BORN}\otimes SM_{LOOP}}$ should include the conterterm contributions as well as the soft and collinear singularity terms coming from the hard emission. We implement this into our monte carlo codes which supply an automatic check of the dependence on these divergence parameters. We can see the UV and IR divergence can be canceled at high precision level in all the phase space, thus leading the continuance of our following calculation.

A Random Phase Space Point for $pp \rightarrow i(p_1)j(p_2) \rightarrow H(p_3)H(p_4), ij = (q\bar{q}, gg)$		
$p_1=(152.42677337684606 \ 0 \ 0 \ 152.42677337684606)$		
$p_2=(152.42677337684606 \ 0 \ 0 \ -152.42677337684606)$		
$p_3=(152.42677337684606 \ 86.461267952196764 \ 0 \ 11.548609707441768)$		
$p_4=(152.42677337684606 \ -86.461267952196764 \ 0 \ -11.548609707441768)$		
divergence	$\sigma_{q\bar{q},gg}^{LED_{BORN}}$	$\sigma_{q\bar{q},gg}^{LED_{BORN}\otimes LED_{LOOP}} + \sigma_{gg}^{LED_{BORN}\otimes SM_{LOOP}}$ [fb]
$\frac{1}{\epsilon_{UV}} = \frac{1}{\epsilon_{IR}^2} = \frac{1}{\epsilon_{IR}} = 0$	0.8461630560055	0.1259656696 911
$\frac{1}{\epsilon_{UV}} = \frac{1}{\epsilon_{IR}^2} = \frac{1}{\epsilon_{IR}} = 10^{10}$	0.8461630560055	0.1259656696 636

Table 1: The UV and IR divergence cancelation at one given random phase space point for the loop contribution. Notice that in the loop terms, we include the conterterm contribution as well as the soft and collinear singularity terms coming from the hard emission contributions.

Since the total cross section is independent of the soft cutoff $\delta_s (= \Delta E_g/E_b, E_b = \sqrt{\hat{s}}/2)$ and the collinear cutoff δ_c , we display the curves of the loop induced QCD corrections to integrated cross section for $pp \rightarrow ij \rightarrow G_{KK} \rightarrow HH + X$ process versus the cutoff δ_s at the $\sqrt{s} = 14$ TeV LHC in the LED model, where we take $\mu_f = \mu_r = \mu_0 = M_H, M_s = 3.5$ TeV, $\delta = 3$ and $\delta_c = \delta_s/100$. For the strong coupling constant $\alpha_s(\mu)$, we use the two-loop evolution of it with the QCD parameter $\Lambda^{n_f=5} = 226$ MeV and get $\alpha_s(\mu_0) = 0.113$. N_f is the number of the active flavors. Some of the LED results are listed in Table 2. The terms gg, uu, dd refer to pure gluon-gluon fusion, $u\bar{u} + c\bar{c}, d\bar{d} + s\bar{s} + b\bar{b}$ collisions respectively. We show the δ_s dependence on all the sub-contribution terms. It is shown clearly that the NLO QCD correction ($\Delta\sigma_{q\bar{q},gg}^{LED_{NLO}}$) does not depend on the arbitrarily chosen values of δ_s and δ_c within the calculation errors. In

δ_s	$\Delta\sigma_{NLO}^{LED}[\text{pb}]$		
	uu	dd	gg
5×10^{-3}	7.843304975113E-03	3.524461919262E-03	1.946637625053E-02
1×10^{-3}	7.846245116613E-03	3.522936306130E-03	1.943421303121E-02
5×10^{-4}	7.846382881667E-03	3.528078248755E-03	1.945856138503E-02
1×10^{-4}	7.846562713918E-03	3.534350158736E-03	1.942754069450E-02
5×10^{-5}	7.844722993687E-03	3.532865728080E-03	1.936325027843E-02
1×10^{-5}	7.793411078227E-03	3.534430130933E-03	1.933905866994E-02

Table 2: The dependence of the loop induced QCD correction to the integrated cross section for the $pp \rightarrow ij \rightarrow G_{KK} \rightarrow HH + X(ij = q\bar{q}, gg)$ at the $\sqrt{s} = 14\text{TeV}$ LHC in the LED model, where we set $\mu_r = \mu_f = \mu_0 = M_H$, $M_s = 3.5\text{TeV}$, $\delta = 3$ and $\delta_c = \delta_s/100$. The terms gg, uu, dd refer to pure gluon-gluon fusion, $u\bar{u} + c\bar{c}$, $d\bar{d} + s\bar{s} + b\bar{b}$ collisions respectively.

the further numerical calculations, we fix $\delta_s = 10^{-4}$ and $\delta_c = \delta_s/100$. To satisfy the unitary constraint, we adopt the cut $\sqrt{\hat{s}} < M_s$ for the whole phase space.

In Fig.5, we show the scale(μ) dependence of the loop induced SM contribution (σ^{SM}), leading order born (σ^{LO}) and QCD loop corrected total (σ^{tot}) cross sections as well as their separate sub-contributions ($\sigma_{q\bar{q}, gg}^{LED}$) in the SM and LED model at the $\sqrt{s} = 14\text{ TeV}$ LHC, and we define the corresponding K-factor as $k_\mu = \sigma^{tot}/\sigma^{LO}$. There we take the input as $M_s = 3.5\text{ TeV}$ and $\delta = 3$. From this figure, we can see:

- For the SM prediction σ^{SM} , see the dot-dashed line in Fig.5, though coming from the SM loop diagrams(Fig.1(a,b,c)), its cross section changes from 44 fb to 20 fb if the scale μ goes from 0.2 to 2 μ_0 , which implies obvious μ dependence.
- For the pure LO and QCD loop induced LED effects, contributions from the gluon fusion (σ_{ggNLO}^{LED}) is about two times of it coming from quark-antiquark collision ($\sigma_{q\bar{q}NLO}^{LED}$). Separately, the $\sigma_{ijNLO}^{LED}(ij = q\bar{q}, gg)$ reduce the μ dependence on the corresponding σ_{ijLO}^{LED} contributions, see the dotted and dashed lines in Fig.5 for more details.
- Sum all the contributions together, we get the μ dependence on the total cross section σ^{LO} and σ^{tot} with the definition in Eq.3.3, see the solid lines in Fig.5. We can see the cross section value in the LED model varies from 95.4(65.9) fb to 48.2(50.9) fb for the LO and NLO contribution when μ goes from 0.2 μ_0 to 2 μ_0 at the $\sqrt{s} = 14\text{ TeV}$ LHC. So that the K-

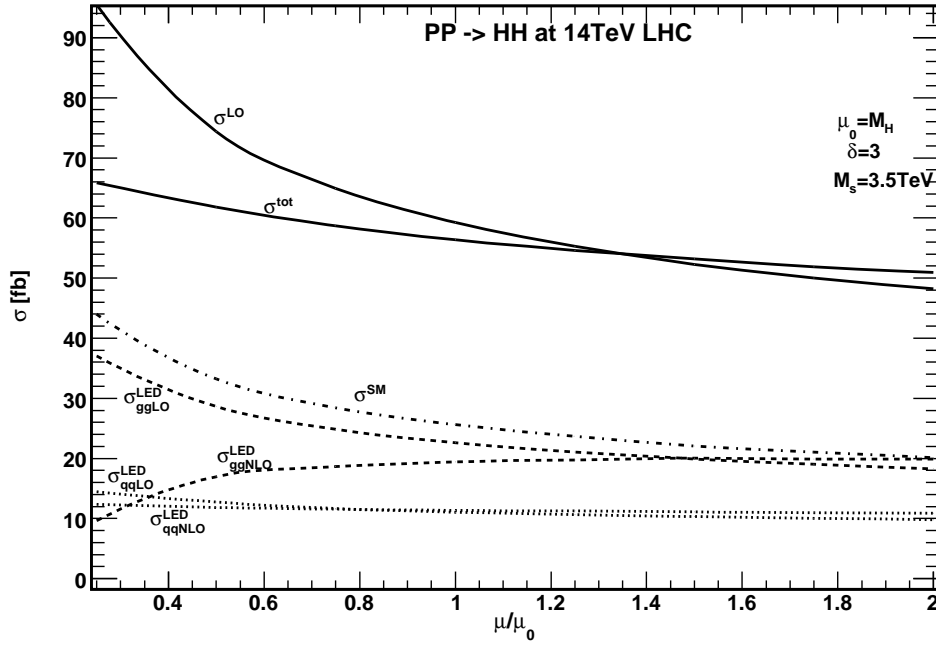


Figure 5: The scale(μ) dependence of the loop induced SM contribution (σ^{SM})[dash-dotted line], leading order born (σ^{LO}) and QCD loop corrected total (σ^{tot})[solid line] cross sections as well as their separate sub-contributions ($\sigma_{q\bar{q},gg}^{LED}$)[dotted and dashed lines] in the SM and LED model at the $\sqrt{s} = 14$ TeV LHC with $\mu = M_H$, $M_s = 3.5$ TeV and $\delta = 3$.

factor in the LED model varies from 1.44871 to 0.946948. We see from this panel that the NLO QCD corrections in the LED model totally reduce the factorization/renormalization scale uncertainty obviously. In further calculations we fix $\mu = \mu_0 = M_H$.

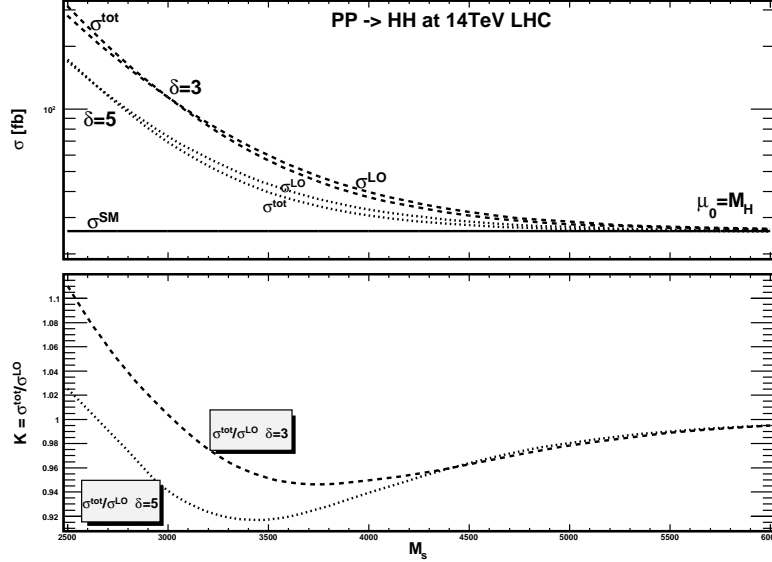


Figure 6: The cross sections and the K-factor(σ^{tot}/σ^{LO}) for the process $pp \rightarrow ij \rightarrow G_{KK} \rightarrow HH + X$ ($ij = q\bar{q}, gg$) in the SM(σ^{SM}) and LED model at both the born(σ^{LO}) level and loop induced level(σ^{tot}) as functions of M_s with $\mu_0 = M_H = 125$ GeV at the $\sqrt{s} = 14$ TeV future LHC. The solid line refer to the SM prediction while the dotted and dashed line correspond to $\delta = 3$ and $\delta = 5$, respectively.

In upper panel of Fig.6, we depict the cross sections for the process $pp \rightarrow ij \rightarrow G_{KK} \rightarrow HH + X$ ($ij = q\bar{q}, gg$) in the SM(σ^{SM}) and LED model at both the tree(σ^{LO}) level and NLO QCD loop induced level(σ^{tot}) as functions of the fundamental scale M_s from 2.5 TeV to 6 TeV with $\mu_0 = M_H = 125$ GeV at the $\sqrt{s} = 14$ TeV future LHC. The solid line presents the SM prediction(σ^{SM}) while the dotted and dashed line correspond to the total LED effects at both the born(σ^{LO}) level and loop induced level(σ^{tot}) with the extra dimension number δ being 3 and 5, respectively. Notice $\sigma^{tot} = \sigma^{SM} + \sigma^{LED}$ and σ^{LO} are defined in Eq.3.3 and Eq.3.8 respectively. From the figures one finds that the largest deviation from the SM due to LED occurs at small values of M_s and δ . With the fixing value of δ , the born level LED effects and the QCD loop induced LED effects deviate at different value of M_s behavior as the dotted and dashed lines presented. In order to compare the relative size of such deviation, we depict the

K-factor(σ^{tot}/σ^{LO}) in the lower panel in Fig.6. One can see for $\delta = 3$, the K-factor is larger than 1 when $M_s < 3$ TeV with the highest value 1.13, while $M_s > 3$ TeV the K-factor can turn to it's lowest value 0.95 which means the loop effects reduce the born effects about 5%. For $\delta = 5$, the K-factor is always less than 1 if $M_s > 2.6$ TeV. When $M_s > 4.5$ TeV, both line close to the the small value of 0.98. The same thing has been depicted in Fig.7 for the 8 TeV early LHC. We take the same input parameters as above, we found that though the LED effects enhance the SM prediction generally, the total loop induced effects reduce the born level LED effects. Their deviation become large if M_s become small and the K-factor turn to their lowest value 0.65 with $M_s = 2.5$ TeV. When M_s become larger then 5 TeV, no matter the value of δ , the K-factor turns to 1 which means the born level and loop induced LED effects become close to each other and also close to their SM predictions.

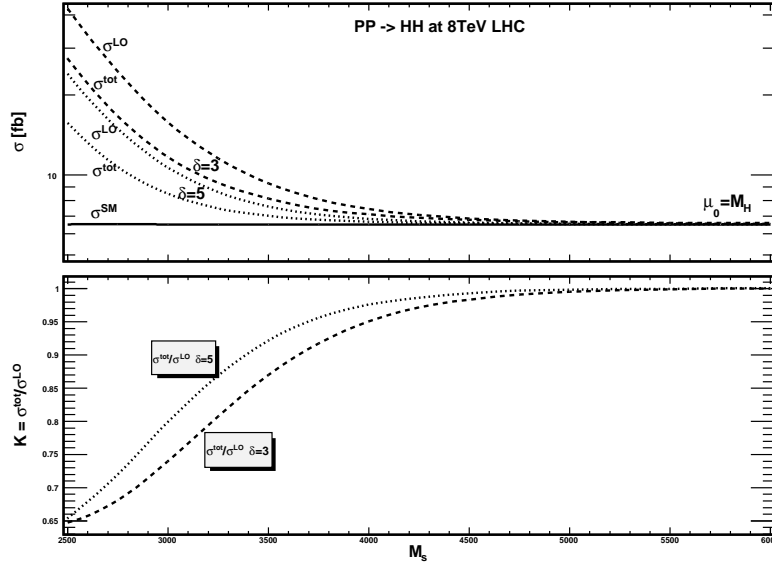


Figure 7: The cross sections and the K-factor(σ^{tot}/σ^{LO}) for the process $pp \rightarrow ij \rightarrow G_{KK} \rightarrow HH + X$ ($ij = q\bar{q}, gg$) in the SM(σ^{SM}) and LED model at both the born(σ^{LO}) level and loop induced level(σ^{tot}) as functions of M_s with $\mu_0 = M_H = 125$ GeV at the $\sqrt{s} = 8$ TeV early LHC. The solid line refer to the SM prediction while the dotted and dashed line correspond to $\delta = 3$ and $\delta = 5$, respectively.

In Fig.8, we show the transverse momentum(p_T)[left panel] and the rapidity(y)[right panel] distributions of the Higgs boson for the process $pp \rightarrow ij \rightarrow G_{KK} \rightarrow HH + X$ ($ij = q\bar{q}, gg$) in the SM($d\sigma^{SM}/dp_T^H$, $d\sigma^{SM}/dy^H$) and LED model($d\sigma^{tot}/dp_T^H$, $d\sigma^{tot}/dy^H$) at the 14 TeV LHC.

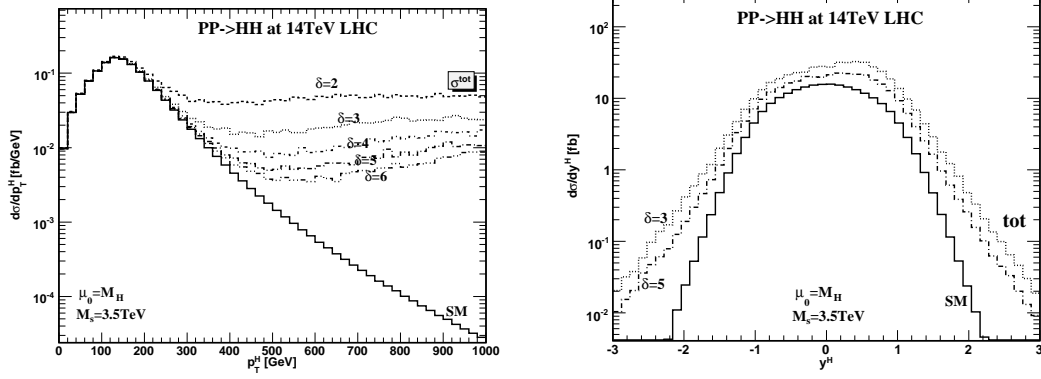


Figure 8: The transverse momentum(p_T)[left panel] and Rapidity(y)[right panel] distribution of Higgs bosons for the process $pp \rightarrow ij \rightarrow G_{KK} \rightarrow HH + X (ij = q\bar{q}, gg)$ at 14 TeV LHC with $M_s = 3.5 TeV$ and $\mu = \mu_0 = M_H$. The solid line presents the SM prediction while the dashed, dotted, dash-dotted and dash-dash-dotted and dash-dash-dot-dotted lines refer to $\delta = 2, 3, 4, 5, 6$, respectively.

There the results are for $M_s = 3.5$ TeV at the fixed value 3 for the number of extra dimensions and obtained by taking the input parameters mentioned above. The LED effects gently raise the SM prediction at values of high p_T^H regions. Rapidity distribution is defined as $\frac{d\sigma}{dy}$ with $\eta = \frac{1}{2} \ln(P_1 \cdot q)/(P_2 \cdot q)$, where P_1 and P_2 are incoming proton momenta and q is the related Higgs boson 4-momenta. As we can see, the rapidity distributions in the LED model show significantly narrow peaks around $y = 0$, which implies the large contributions at high p_T region.

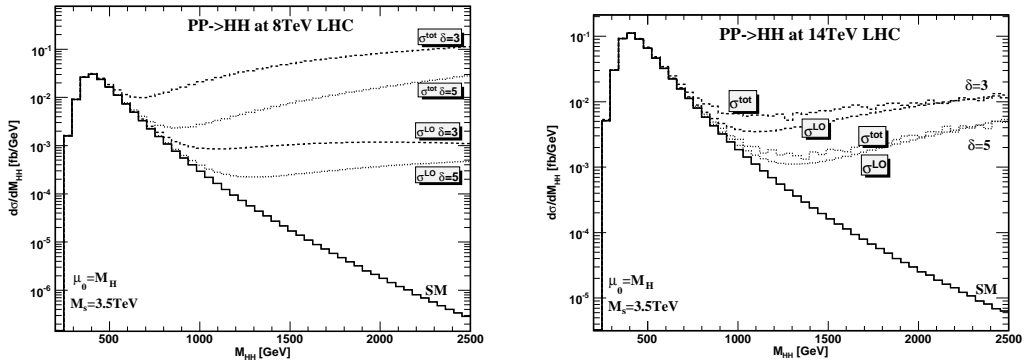


Figure 9: The invariance mass(M_{HH}) distribution of Higgs boson pair for the process $pp \rightarrow ij \rightarrow G_{KK} \rightarrow HH + X (ij = q\bar{q}, gg)$ at 8TeV[left panel] and 14 TeV[right panel] early and future LHC with $M_s = 3.5 TeV$ and $\mu = M_H$. The solid line presents the SM prediction while the dashed, dotted lines refer to $\delta = 3, 5$, respectively. The upper one refer to σ^{tot} while the lower one refer to σ^{LO} .

The distributions of the invariance mass(M_{HH}) distribution of Higgs boson pair for $pp \rightarrow ij \rightarrow G_{KK} \rightarrow HH + X (ij = q\bar{q}, gg)$ has been displayed in Fig.9 at the 8 TeV[left panel] and 14 TeV[right panel] early and future LHC. Same conclusion can be obtained that the LED effects enhance the distribution at the high M_{HH} region since in these regions the LED effect dominant the total (SM+LED) distribution, as a result, more KK modes contribute with the increase of M_{HH} . The lower the dimension is, the higher value of M_{HH} deviation from its SM prediction as presented in Fig.9. It will be also very interesting to compare the results at 8 TeV with that at 14 TeV LHC. We can see that though 14 TeV LHC has much higher c.m.s. energy than 8 TeV LHC, the theoretical amplitude at higher c.m.s. LHC is hampered by the unitary constraint $\sqrt{\hat{s}} < M_s$, thus the LED effect is much suppressed at 14TeV LHC than 8 TeV LHC. Besides, at the 8 TeV LHC, the total contribution σ^{tot} deviate from its leading order contribution σ^{LO} obviously. The deviations become much larger compare to the 14 TeV results. While at 14 TeV LHC, the deviations only appear in the middle of M_{HH} region between σ^{tot} and σ^{LO} when the dimension is fixed to be the same value.

As have been told, the distribution shows the crucial character that the LED effects are mainly collected at high p_T^H and M_{HH} region while the SM backgrounds are leaving in the lower regions. We thus apply two strict cuts $p_T(H) \geq 500$ GeV and $M_{HH} \geq 1$ TeV to strongly suppress the SM backgrounds while leaving the LED effects almost unchanged. We concentrate on two channels: $pp \rightarrow HH \rightarrow b\bar{b}\gamma\gamma$ and $pp \rightarrow HH \rightarrow b\bar{b}\mu^-\mu^+$. The main backgrounds come from $pp \rightarrow ZZ(ZH)$ (with $Z \rightarrow b\bar{b}(\mu^-\mu^+)$ can be a background to $h \rightarrow b\bar{b}(\mu^-\mu^+)$) and $pp \rightarrow t\bar{t} \rightarrow b\bar{b}\mu^-\mu^+\nu\bar{\nu}$. By taking into account all these backgrounds and adopting the kinematic cuts mentioned above, we display the signal background ratio $\frac{S}{\sqrt{B}}$ in Table3 and Table4 corresponding to the two different decay channels with M_s and δ as running parameter and luminosity equal (100, 600)[fb^{-1}] at 14 TeV future LHC. From these two tables we can see that Higgs pair production in LED model can give significant signal to background ratio when the scale $M_s \leq 5$ TeV and dimension $\delta \leq 5$. By using the $b\bar{b}\gamma\gamma$ channel, one can test LED effects at $M_s = 5$ TeV and $\delta = 4$ with $\frac{S}{\sqrt{B}} > 3$ while for $b\bar{b}\mu^-\mu^+$ channel with $\frac{S}{\sqrt{B}} \geq 5$. Both channels shows good character in testing LED effects. In the tables, $\sim (<)1$ means the $\frac{S}{\sqrt{B}}$ is

$\frac{S}{\sqrt{B}}$	$b\bar{b}\gamma\gamma$ channel @ 14 TeV with $\mathcal{L}=(100, 600)[fb^{-1}]$									
$M_s[\text{TeV}]$	$\delta = 2$		$\delta = 3$		$\delta = 4$		$\delta = 5$		$\delta = 6$	
3.5	26	64	12.4	30	11	26	8.2	20	6.5	16
4.0	11.2	27.4	6.4	15.6	4.4	11	3.1	7.5	2.6	6.3
4.5	5.2	13	2.8	6.8	1.9	4.5	1.4	3.3	1.1	2.6
5.0	2.5	6.1	1.8	4.2	1.3	3.2	~ 1	1.5	~ 1	1.2
5.5	1.3	3.2	~ 1	1.5	< 1	1	< 1	~ 1	< 1	~ 1

Table 3: $\frac{S}{\sqrt{B}}$ for the channel $pp \rightarrow HH \rightarrow b\bar{b}\gamma\gamma$ after taking into account all backgrounds and adopt the kinematic cuts.

$\frac{S}{\sqrt{B}}$	$b\bar{b}\mu^-\mu^+$ channel @ 14 TeV with $\mathcal{L}=(100, 600)[fb^{-1}]$									
$M_s[\text{TeV}]$	$\delta = 2$		$\delta = 3$		$\delta = 4$		$\delta = 5$		$\delta = 6$	
3.5	60	146	29	70	25	61	19	46	15	37
4.0	26	64	15	36	10	25	8	18.4	6	14.4
4.5	12	29	7	16	4.2	10.3	3.2	8	3	6
5.0	6	14	4	7.3	2	5	1.4	3.4	1.1	3
5.5	3	7	2	4	1	2.2	~ 1	1.4	~ 1	1.2

Table 4: $\frac{S}{\sqrt{B}}$ for the channel $pp \rightarrow HH \rightarrow b\bar{b}\mu^-\mu^+$ after taking into account all backgrounds and adopt the kinematic cuts.

close to (less than) 1, however, this can be improved if we apply the cuts more strict or wait for the luminosity to be higher at the LHC. It will be interesting that $pp \rightarrow G_{KK} \rightarrow HH$ can also be a promising process in testing LED effects.

V. Summary

In this work, we present the a full treatment of the QCD loop induced corrections to the 125 GeV neutral Higgs pair production process $pp \rightarrow ij \rightarrow G_{KK} \rightarrow HH + X$ ($ij = q\bar{q}, gg$) at the early ($\sqrt{s} = 8$ TeV) and future ($\sqrt{s} = 14$ TeV) LHC in the context of large-extra-dimensions(LED) model including the Kaluza-Klein(KK) excited gravitons. We investigate the dependence of the total corrected cross sections on the renormalization/factorization scale μ , and study the corrected distributions of the transverse momenta(p_T^H), invariant mass(M_{HH}) and rapidity(y^H) distributions. Our final results show that the LED model raises the cross section of Higgs pair production compare to its SM prediction and enhance the transverse momentum(p_T^H) and distributions at high scales of p_T^H and M_{HH} . By including the QCD loop corrections, the scale

dependence of total cross section can be reduced obviously. Choose decay modes like $HH \rightarrow b\bar{b}\gamma\gamma$ or $HH \rightarrow b\bar{b}\mu^-\mu^+$ and some simple cuts, we can strongly reduce the SM background but keep most of the LED effects leading Higgs pair production a promising channel to search for LED effects.

Acknowledgments: We would like to thank Zhang Ren-You and Li Hong-Lei for useful discussions. Project supported by the National Natural Science Foundation of China (Grant No.11147151, No.11205070, No.11105083, No.10947139 and No.11035003), and by Shandong Province Natural Science Foundation (No.ZR2012AQ017).

References

- [1] N. Arkani-Hamed, S. Dimopoulos and G. R. Dvali, Phys. Lett. B **429**, 263 (1998) [hep-ph/9803315]; N. Arkani-Hamed, S. Dimopoulos and G. R. Dvali, Phys. Rev. D **59**, 086004 (1999) [hep-ph/9807344].
- [2] D. J. Kapner, T. S. Cook, E. G. Adelberger, J. H. Gundlach, B. R. Heckel, C. D. Hoyle and H. E. Swanson, Phys. Rev. Lett. **98**, 021101 (2007) [arXiv:hep-ph/0611184].
- [3] T. Plehn, M. Spira, and P.M. Zerwas, Nucl. Phys. B479, 46 (1996); Erratum, ibid. B531, 655 (1998).
- [4] U. Baur, T. Plehn and D. L. Rainwater, Phys. Rev. D 68, 033001 (2003); Phys. Rev. D 69, 053004 (2004).
- [5] M. J. Dolan, C. Englert and M. Spannowsky, arXiv:1206.5001 [hep-ph].
- [6] Hao Sun, Wen-Gan Ma, Ya-Jin Zhou, Yan-Bin Sun, Ren-You Zhang and Hong-Sheng Hou, Commun.Theor.Phys.41:73-78(2004).
- [7] Lei Wang, Wenyu Wang, Jin Min Yang, Huanjun Zhang, Phys.Rev.D76, 017702 (2007).
- [8] Hiroshi de Sandes, Rogerio Rosenfeld, Phys.Lett.B659, 323-327 (2008).
- [9] C. S. Kim, Kang Young Lee and Jeonghyeon Song, Phys.Rev.D64:015009(2001).

- [10] Gian F. Giudice, Riccardo Rattazzi, James D. Wells, Nucl.Phys. B544, 3-38 (1999).
- [11] Tao Han, Joseph D. Lykken, Ren-Jie Zhang, Phys.Rev.D59:105006(1999).
- [12] J. L. Hewett, Phys. Rev. Lett. 82 (1999) 4765; Prakash Mathews, V. Ravindran, K. Sridhar and W. L. van Neerven, Nucl. Phys. B713 (2005) 333; Prakash Mathews, V. Ravindran, Nucl. Phys. B753 (2006) 1; M.C. Kumar, Prakash Mathews, V. Ravindran, Eur. Phys. J. C49 (2007) 599.
- [13] O. J. P. Eboli, Tao Han, M. B. Magro, P. G. Mercadante, Phys. Rev. D61 (2000) 094007; K.m. Cheung and G. L. Landsberg, Phys. Rev. D 62 (2000) 076003; M.C. Kumar, Prakash Mathews, V. Ravindran, Anurag Tripathi, Phys. Lett. B672 (2009) 45; Nucl. Phys. B818 (2009) 28.
- [14] M. Kober, B. Koch and M. Bleicher, Phys. Rev. D **76**, 125001 (2007) [arXiv:0708.2368]; J. Gao, C. S. Li, X. Gao and J. J. Zhang, Phys. Rev. D **80**, 016008 (2009) [arXiv:0903.2551]; Neelima Agarwal, V. Ravindran, V. K. Tiwari, Anurag Tripathi, Nucl. Phys. B830 (2010) 248.
- [15] Z. U. Usuhov and I. A. Minashvili, Phys. Part. Nucl. Lett. **3**, 153 (2006) [Pisma Fiz. Elem. Chast. Atom. Yadra **3**, 24 (2006)]; K. Y. Lee, H. S. Song and J. -H. Song, Phys. Lett. B **464**, 82 (1999) [hep-ph/9904355]. Neelima Agarwal, V. Ravindran, V. K. Tiwari, Anurag Tripathi, Phys. Rev. D82 (2010) 036001; B. Yu-Ming, G. Lei, L. Xiao-Zhou, M. Wen-Gan and Z. Ren-You, Phys. Rev. D **85**, 016008 (2012) [arXiv:1112.4894].
- [16] Prakash Mathews, Sreerup Raychaudhuri, K. Sridhar, Phys. Lett. B450(1999) 343; JHEP 0007 (2000) 008.
- [17] K. Y. Lee, H. S. Song, J. -H. Song and C. Yu, Phys. Rev. D **60**, 093002 (1999) [hep-ph/9905227]; K. Y. Lee, S. C. Park, H. S. Song, J. -H. Song and C. Yu, Phys. Rev. D **61**, 074005 (2000) [hep-ph/9910466]; hep-ph/0105326; S. C. Inan and A. A. Billur, Phys. Rev. D **84**, 095002 (2011).
- [18] Hao Sun, Ya-Jin Zhou, He Chen, Eur. Phys. J. C (2012) 72:2011.

- [19] C. Collaboration [CMS Collaboration], arXiv:1204.0821 [hep-ex].
- [20] S. Chatrchyan *et al.* [CMS Collaboration], Phys. Lett. B **711**, 15 (2012) [arXiv:1202.3827 [hep-ex]].
- [21] S. Chatrchyan *et al.* [CMS Collaboration], arXiv:1112.0688 [hep-ex].
- [22] Roberto Franceschini, Gian Francesco Giudice, Pier Paolo Giardino, Paolo Lodone, Alessandro Strumia, JHEP 1105, 092 (2011).
- [23] ATLAS Collaboration, ATLAS-CONF-2011.163
- [24] CMS Collaboration, CMS PAS HIG-11-032
- [25] Bai Yu-Ming, Guo Lei, Li Xiao-Zhou, Ma Wen-Gan, Zhang Ren-You, Phys. Rev. D85(2012) 016008.
- [26] Marco Guzzi, Pavel Nadolsky, Edmond Berger, Hung-Liang Lai, Fredrick Olness, C.-P. Yuan, SMU-HEP-10-11, [arXiv:1101.0561].
- [27] S. Kawabata, Comp. Phys. Commun. 88, 309 (1995). F. Yuasa, D. Perret-Gallix, S. Kawabata, and T. Ishikawa, Nucl. Instrum. Meth. A389, 77 (1997).
- [28] Hameren A van arXiv:1003.4953[hep-ph].
- [29] B. W. Harris and J. F. Owens, Phys. Rev. D **65**, 094032(2002).
- [30] T. Hahn, Comput.Phys.Commun. 140, 418-431 (2001).
- [31] T. Hahn, Nucl.Phys.Proc.Suppl. 89, 231-236 (2000).
- [32] T.Hahn,M.Perez-Victoria,Comput.Phys.Commun.118:153-165(1999).
- [33] A. van Hameren, Comput.Phys.Commun.182:2427-2438,2011.
- [34] A. Djouadi, J. Kalinowski and M. Spira, Comput. Phys. Commun. 108, 56 (1998).
- [35] Particle Data Group, K. Nakamura et al., JPG **37**, 075021 (2010).
- [36] U. Baur, T. Plehn and D. Rainwater, Phys. Rev. D 68, 033001 (2003).